Published in final edited form as:
Curr Opin Chem Biol. 2010 February ; 14(1): 97. doi:10.1016/j.cbpa.2009.10.009.

Functionalized ^{129}Xe contrast agents for magnetic resonance imaging

Olena Taratula and **Ivan J. Dmochowski***
Contribution from the Department of Chemistry, University of Pennsylvania, 231 South 34th St., Philadelphia, PA 19104-6323

Olena Taratula: otaratula@gmail.com; Ivan J. Dmochowski:

Abstract

The concept of 'xenon biosensor' for magnetic resonance imaging (MRI) was first proposed by a Berkeley team in 2001, with evidence that hyperpolarized ^{129}Xe bound to a biotin-labeled cryptophane can detect streptavidin at much lower concentrations (nM-μM) than is typical for contrast-enhanced MRI experiments. ^{129}Xe biosensors have undergone many recent developments to address challenges in molecular imaging. For example, cryptophanes have been synthesized that exhibit 10-fold higher xenon affinity with distinct ^{129}Xe magnetic resonance spectra. Also relevant are dendrimeric cryptophane assemblies and inorganic zeolites that localize many ^{129}Xe atoms to rare targets. Finally, this article considers biosensors that produce measurable changes in ^{129}Xe chemical shift based upon the activity of oligonucleotides, proteins, or enzymes, and includes the first cell studies.

Introduction

Hyperpolarized (hp) ^{129}Xe biosensors were introduced in 2001 as novel contrast agents for magnetic resonance imaging (MRI) and spectroscopy (MRS) [1]. Xenon biosensors put a new (nuclear) spin on an old story: In 1973, Lauterbur [2] and Mansfield [3] obtained the first MR images from free induction decay (FID) data acquired in the presence of magnetic field gradients. Today, noninvasive proton (^{1}H) MRI is one of the most widely used and versatile techniques for scanning deep tissue in the diagnosis of human disease. However, intrinsic ^{1}H MRI signals typically provide poor detection sensitivity. Consequently, contrast agents must be introduced into patients for image enhancement, as occurs in more than half of the roughly 30 million MRI procedures performed annually in the U.S.

Contrast media based on gadolinium or iron-oxide particles have been reviewed extensively [4–5]. Efforts to enhance contrast further have produced 'smart' Gd^{3+} [6], iron-oxide [7], and also ^{19}F-based agents [8] that provide signal in response to a biological trigger. However, fundamental limitations in sensitivity have motivated the investigation of alternate nuclei such as ^{129}Xe, ^{13}C, ^{83}Kr, and ^{3}He [9–12], which can be hyperpolarized to produce unpaired spins that result in much larger NMR signal.

*Corresponding author: Dmochowski, Ivan, ivandmo@sas.upenn.edu, Fax: 215-573-6329.

Here, we focus on molecular imaging with ^{129}Xe gas, which is spin-½ and can achieve a hyperpolarized state with spin-lattice relaxation time (T_1) of roughly 70 min. 129Xe hyperpolarization yields ~10^5 signal enhancement relative to the normal Boltzmann distribution of nuclear spins. The process of generating hp ^{129}Xe through spin-exchange optical pumping (Figure 1A) [13] involves the transfer of angular momentum from circularly polarized light to an alkali metal (here we consider Rb). Polarized Rb subsequently interacts with the nuclear spin of xenon through dipolar coupling. Recently, large improvements in ^{129}Xe hyperpolarization technology have achieved > 50% hp ^{129}Xe at flow rates of 1–2 L per min, which enables human clinical applications [14].

Hyperpolarized ^{129}Xe offers potential advantages over conventional MRI contrast agents, namely: roughly 10^4–fold more NMR signal per nucleus than a corresponding proton, which takes into account the greater gyromagnetic ratio and isotopic abundance of ^{1}H relative to ^{129}Xe; lower toxicity than Gd^{3+} and most other paramagnetic metal ions, as xenon has low affinity for proteins and is relatively ‘inert’ in the body when introduced below the anesthetic threshold, which is 70% by volume of inhaled gas mixtures; exquisite NMR chemical shift sensitivity, with a greater than 200 ppm spectral window in aqueous solution, which facilitates the detection of multiple species simultaneously (i.e., multiplexing); and, significant polarizability, which contributes to xenon’s millimolar solubility in water [15] and promotes binding to molecular hosts via London dispersion forces. ^{129}Xe biosensors (Figure 1B) that exploit xenon’s unique physical properties create exciting opportunities for molecular imaging. This article focuses on very recent advances in xenon biosensor design and application.

Xenon Biosensing: The Host Molecule

We define ‘xenon biosensor’ simply as a xenon-encapsulating agent attached to one or more bioactive molecules. Due to its filled valence electron shell, xenon resists forming covalent bonds; nonetheless, it shows modest affinity for hydrophobic cavities found in many organic molecules [16–19]. For example, the association constant, K_A, is 200 M^{-1} for hemicarcerands [20] and 20 M^{-1} for α-cyclodextrin [17]. A calix[4]arene derivative exhibited a K_A of only ~14 M^{-1} at 298 K in water [21] whereas for water-soluble cucurbit[6]uril, a xenon binding constant of 3000 M^{-1} was measured [18]. In fact, the non-covalent, dynamic association of ^{129}Xe with these host molecules creates opportunities for xenon biosensing applications, as xenon can be hyperpolarized separately as the gas and subsequently introduced to the host molecule, at multiple time points for longitudinal studies.

Cryptophane-A, first reported in 1981 [22], is the most studied Xe-binding cage and is comprised of two cyclotriveratrylene caps joined by three ethyl linkers, which give an internal van der Waals volume of approximately 95 $Å^3$ (Figure 2). As a result of its connectivity, cryptophane-A has D3 symmetry and is chiral. Cryptophane-A is also commonly referred to as cryptophane-2,2,2, based on the three 2-carbon spacers. Cryptophane-A binds Xe reversibly with $K_A \sim 3{,}900\ M^{-1}$ in $C_2D_2Cl_4$ at 278 K [23]. In a series of related cryptophanes incorporating 3-carbon spacers, xenon affinity decreases with increasing size of the cavity [24].

Cryptophane-1,1,1 was recently synthesized [25], and exhibits the highest Xe association constant measured in organic solvent, K_A = 10,000 M^{-1} at 293 K. This host has a calculated internal volume of 81 $Å^3$, making the xenon volume (42 $Å^3$) to host ratio equal to 0.52, which is very close to Mecozzi and Rebek’s prescribed 0.55 ratio for nonpolar host-guest complexes mediated purely by London forces [26]. Cryptophane-1,1,1 shows very slow decomplexation kinetics, which produces a narrow ^{129}Xe NMR resonance useful for direct detection, but also hinders the Xe exchange needed for indirect detection [27]. As this example shows, both thermodynamics and kinetics impact the design of host molecules for xenon biosensing applications.

Several water-soluble cryptophanes have been synthesized to date, many with exceptional xenon-binding characteristics [28–30]. Huber's water-soluble cryptophanes [28] replaced all six methoxy groups with OCH_2COOH. The Xe affinity of hexa-acid cryptophane-A was measured to be 6800 M^{-1} at 293 K. Conformational changes were observed in the hexa-acid cryptophanes, including a non-xenon-binding crown-saddle isomer. Our lab subsequently developed synthetic protocols for attaching three carboxylates on just one of the cyclotriveratrylenes [29]. This creates a dipole moment along the axis of the cage that may interact favorably with the xenon electron cloud.

In order to perform more accurate and rapid measurements of xenon binding, our lab developed fluorescence quenching and isothermal titration calorimetry (ITC) assays [30]. Reacting tri-propargyl cryptophane with three azido-propionates gave a water-soluble cryptophane with association constant of 1.7×10^4 M^{-1} at 293 K [29]. ITC indicates that entropy is an important factor in aqueous xenon binding, as $-T\Delta S$ is of similar magnitude to ΔH. As a result, xenon affinity increases with temperature: $K_A = 3.0 \times 10^4$ M^{-1} at 310 K. Importantly, xenon binding studies with the same compound in human plasma showed similar affinity ($K_A = 2.2 \times 10^4$ M^{-1} at 310 K), which supports use of cryptophanes for cellular imaging. In order to improve xenon binding further, a cryptophane was synthesized with the carboxylates placed closer to the cavity [30]. Presently, a tri-acetate cryptophane-A shows the highest affinity for xenon of any host molecule in water, $K_A = 3.3 \times 10^4$ M^{-1} at 293 K.

Importantly for multiplexing studies, the known cryptophanes produce very different ^{129}Xe NMR chemical shifts [25,28,31]. Among Huber's hexa-acid cryptophanes in water, the encapsulated ^{129}Xe shows a single resonance that shifts ~30 ppm upfield with increasing size of the cavity: 222-cage, 64 ppm; 223-cage, 52 ppm; 233-cage, 42 ppm; 333-cage, 35 ppm [28]. A similar trend is observed for the corresponding organic-soluble cryptophanes in $C_2D_2Cl_4$ [13]. This range of chemical shifts will enable multiplexing experiments that employ different cryptophanes to target various biomarkers. Furthermore, these data suggest that as the cavity becomes smaller, the electron cloud of the xenon feels a greater perturbation from the cage, leading to a larger chemical shift. Interestingly, the Xe@cryptophane-1,1,1 peak is at 31.1 ppm, fully 36 ppm *upfield* from Xe@cryptophane-2,2,2 in $C_2D_2Cl_4$. Although this appears to violate the volume-chemical shift trend, cryptophane-1,1,1 lacks the six methoxy substituents on the phenyl rings. This suggests that incorporating electron-donating and withdrawing substituents on the cryptophane should allow efficient stereoelectronic modulation of ^{129}Xe NMR chemical shift for molecular imaging applications.

Xenon Biosensing: The Targeting Molecule

Attached to the host is the targeting molecule, which may be a recognition moiety with high affinity and specificity for a single analyte, e.g., biotin-streptavidin [1,32], peptide-antigen [33], DNA-DNA hybrid [34], or affinity tag for a specific cancer biomarker [35–36]. Attachment of a substrate molecule has the potential to allow even more sensitive detection of an enzyme via the conversion of multiple substrates to products [37]. However, activity-based enzyme sensors must ensure that ^{129}Xe is sufficiently near to the substrate to detect product formation. By the same token, the host molecule should not interfere with enzyme activity.

A ^{129}Xe-biosensor complex freely diffusing in solution typically results in a single NMR resonance (Figure 1B) that does not distinguish between cryptophane enantiomers. Binding to a biological receptor typically produces one or more additional ^{129}Xe peaks. To date, many xenon biosensors have relied on a monofunctionalized cryptophane approach [32–33,35,37]. Newer approaches for tri-substituting cryptophane-A facilitate the introduction of additional targeting moieties, water solubilizing groups or dye labels for fluorescence microscopy (Figure

2) [30,36]. Such flexibility is useful for tuning the biological and spectroscopic properties of the xenon biosensor.

Hyperpolarized ^{129}Xe Biodetection: Overview

It is now possible to collect MR images of inhaled hp ^{129}Xe in the lungs, brain, and other organs of the body [38–41]. However, ^{129}Xe MRI biosensors will require even greater sensitivity to achieve *in vivo* molecular imaging. Two different biodetection strategies are possible: 1) Target localization, with maximal hp ^{129}Xe localized to the target and minimal background signal elsewhere in the specimen; 2) Multiplexing, whereby multiple xenon biosensors identify several biomarkers. Colocalization of different ^{129}Xe MR spectroscopic signals should help to identify unusual cellular biochemistry, as might be associated with a disease state.

Xenon delivery strategies have sought to maximize the signal-to-noise ratio of the hyperpolarized ^{129}Xe MR signal, by minimizing the decay of polarization during transport or by dilution [38,42]. The T_1 of ^{129}Xe varies widely in solution, depending on its molecular environment [1,43–46]: T_1 = 4 s in deoxygenated blood, T_1 = 13 s in oxygenated blood, T_1 = 20–40 s in cryptophanes, and $T_1 \approx 1000$ s in deuterated saline solution [43,47]. Direct inhalation is the most clinically feasible method of delivering hyperpolarized ^{129}Xe in humans, and some organs, such as the lungs and brain are accessible in this way [48]. In other cases, direct intravenous [42] or arterial [38] injection of hyperpolarized ^{129}Xe is feasible, particularly in rodents. Thus, it is practical to deliver hp ^{129}Xe for sensitive *in vivo* MRI detection following introduction of the biosensor. Experiments with radioisotope ^{133}Xe in pigs confirmed that xenon is cleared from the lungs and other organs, with retention only in fatty tissues after two hours [49]. Thus, introduction of fresh hp ^{129}Xe will allow longitudinal studies, provided the biosensor is retained.

Hyperpolarized ^{129}Xe Biodetection: Synthetic Strategies

Water-soluble dendrimers have been shown to encapsulate multiple cryptophanes, while presenting recognition moieties that deliver the cargo to a specific target [50]. The published approach exploited electrostatic and hydrophobic interactions to incorporate the cryptophanes, which avoided synthetic steps and the creation of cryptophane diastereomers that might produce additional ^{129}Xe NMR resonances. This invites exploration of polymeric systems that carry a larger payload of cryptophane and improve bioavailability. Relevant examples are micelles and liposomes that can enhance MRI contrast by encapsulating large numbers of paramagnetic species [51].

Another interesting approach for localizing xenon is the use of nanoporous materials. Lerouge prepared silica-based, 65-nm zeolites that contained many pores capable of binding hp ^{129}Xe with a fairly long T_1 [52]. Biocompatibility and colloidal stability of these nanoparticles were achieved by functionalization with PEG chains and a peptide targeting biological receptors; localization in a mouse was studied by ^{111}In scintigraphy. It may be possible to create zeolite structures with enhanced xenon-binding and spectroscopic characteristics, as needed for hp ^{129}Xe MRI studies.

Hyperpolarized ^{129}Xe Biodetection: NMR Strategies

Sensitive NMR methods for detecting hp ^{129}Xe have been developed, as elaborated in a recent review [53]. Most promisingly, a hp ^{129}Xe chemical exchange saturation transfer (hyper-CEST) strategy allows the selective depolarization of biosensor-bound hp ^{129}Xe using pulsed excitation [27]. This leads to the accumulated depolarization of bulk hp ^{129}Xe through rapid exchange of xenon atoms between “cryptophane-bound” and “free” states. Monitoring depletion of the “free” hp ^{129}Xe NMR signal provides roughly 10^3 signal enhancement, based

on the large pool of aqueous xenon (~ 3 mM at 1 atm and 310 K) [15] compared to the typically micromolar concentration of ^{129}Xe@biosensor that can be delivered to cells and other biological targets. However, some challenges remain. For example, it will be difficult to achieve a constant polarization level *in vivo*. Moreover, a decrease of spatial resolution is likely, due to xenon diffusion during the long saturation time.

Biological Applications: Achieving Large ^{129}Xe NMR Chemical Shifts

The initial Berkeley biotin biosensor gave a hp ^{129}Xe NMR peak at 70 ppm. Addition of 40 nanomoles of streptavidin produced a new hp ^{129}Xe NMR peak ~2.5 ppm downfield [1]. Shorter tethers that enforce the streptavidin-cryptophane interaction shifted the ^{129}Xe NMR spectrum by as much as 4 ppm [54–56]; however, the ^{129}Xe NMR resonances also became considerably broadened (> 1 ppm), which limited biodetection. The origin of the ^{129}Xe NMR chemical shift, as well as the appearance of multiple “bound” peaks in some systems, have been investigated computationally by Jameson [55,57]. It is now evident that cryptophane-biotin diastereomers can produce overlapping ^{129}Xe NMR spectra. An additional complication is that streptavidin (a dimer of dimers) binds multiple biotins, which may promote Xe-cryptophane:Xe-cryptophane interactions.

We subsequently designed an enzyme-responsive ^{129}Xe biosensor for the detection of a cancer biomarker, matrix metalloproteinase-7 [37]. The probe was designed such that proteolysis of a peptide containing three positively charged residues caused a change in the electrostatic environment of ^{129}Xe, which could possibly affect ^{129}Xe NMR chemical shift. ^{129}Xe NMR peaks of 61.9 and 62.5 ppm for the intact peptide diastereomers gave upfield shifts of 0.5 and 0.3 ppm upon proteolysis. Although these $\Delta\delta$ values are too small for *in vivo* detection, this work illustrated the potential for studying enzyme activity.

Roy et al. subsequently designed a cryptophane biosensor for *in vitro* DNA detection [34]. In order to avoid formation of diastereomers, a chiral (−)-cryptophane-A was synthesized and covalently attached to a 20-mer DNA probe. The NMR spectrum of hp ^{129}Xe with this biosensor alone or in the presence of noncomplementary DNA gave a peak at 68.5 ppm. Addition of the complementary DNA strand produced a new resonance at 67.0 ppm that clearly identified the DNA target in solution. Although unique DNA sequences are rare targets in the cell nucleus, this illustrates the utility of enantiopure cryptophanes for biosensing applications. More recently, Schlundt introduced a peptide-labeled ^{129}Xe biosensor that binds to a major histocompatibility complex (MHC) class II protein [33]. In this case, a 1-ppm downfield shift was observed upon protein binding, and larger chemical shift changes may be possible using a shorter linker. This work demonstrated sensitive biodetection using hyper-CEST NMR techniques.

Finally, our lab has developed ^{129}Xe biosensors for a second cancer biomarker, carbonic anhydrase (CA), which serves as a useful model system for elucidating the origin of ^{129}Xe NMR chemical shifts [36]. Tri-propargyl cryptophane was substituted with linkers varying between 6 and 8 bonds to CA-specific *p*-benzenesulfonamide ligand to yield non-diastereomeric biosensors with a single ^{129}Xe NMR resonance. These Xe biosensors were designed to bind CA isozymes I and II by considering the depth of the active-site channel, the size of the cryptophane, and the propensity of related compounds to bind CA. X-ray crystallographic studies confirmed binding of benzenesulfonamide to Zn^{2+} at the CAII active site (Figure 3A), with the 8-bond-linked cryptophane positioned at the mouth of the protein channel [58].

The biosensors complexed with CA I and II yielded “bound” hyperpolarized ^{129}Xe NMR resonances of narrow linewidth at approximately 64 ppm that were shifted between 3.0 and 7.5 ppm downfield upon CA binding. These chemical shift differences clearly distinguished

between CA I and II in solution. One of the most intriguing findings from this work came with the 7-bond-linker biosensor, which showed one “bound” resonance for CAI and distinctively two “bound” resonances for CAII (Figure 3B).

Biological Applications: Xenon Biosensors in Cells

Our lab has synthesized Xe biosensors targeting cancer biomarkers and performed cell studies [35]. Mono-propargyl cryptophane reacted with azido-peptides in a copper(I)-catalyzed [3+2] cycloaddition. Delivery of cryptophane into human cancer and normal cell lines was achieved with cationic cell penetrating peptides. A tetraRGD peptide targeting $\alpha_v\beta_3$ integrin increased specificity of cryptophane cell uptake (Figure 4). The peptido-cryptophanes were determined to be relatively nontoxic at the micromolar concentrations needed for hp ^{129}Xe NMR experiments.

Conclusion: A Bright and Undetermined Future for ^{129}Xe MRI Biosensing

^{129}Xe MRI biosensors have been designed to bind xenon with high affinity and target oligonucleotides or proteins [33–34,36–37]. Such compounds have the potential to detect various diseases, by localizing hp ^{129}Xe to a tissue and/or by providing multiplexed detection of different biomarkers. Improved capabilities for hp ^{129}Xe detection and chemical shift resolution are also coming from new ^{129}Xe hyperpolarization technology [13], organic and inorganic assemblies for localizing large numbers of ^{129}Xe atoms [50,52], and hyper-CEST imaging strategies [27]. Uptake of xenon biosensors in cells and mice has been verified [35, 52]. In addition, proof-of-concept MRI studies have demonstrated the ability to resolve spatially cryptophanes that are targeted to labeled beads, different compartments or solvents [27,59–61]. Intravenously injected hp ^{129}Xe-saturated saline was shown to be a useful probe for pulmonary perfusion or gas exchange evaluation in the lung [62], further validating ^{129}Xe MRI as a sensitive method for imaging lung diseases [63]. With these rapid technological advances, it should now be possible to detect specific bio-receptors in cells and animals via contrast-enhanced hp ^{129}Xe MRI and MRS. Experimental validation appears to be close at hand, which will guide the continued development of xenon biosensors for molecular imaging and help to identify the best *in vivo* applications for this technology.

Acknowledgments

We acknowledge our colleagues and researchers world-wide for their contributions to the field of xenon biosensing. Special thanks go to Julie Aaron for supplying Figure 3A. Work on this manuscript was supported by the DOD (W81XWH-04-1-0657), NIH (1R33CA110104), and Camille and Henry Dreyfus Teacher-Scholar Award to I.J.D.

References and recommended reading

Recent papers of particular interest are highlighted as:

• of special interest

•• of outstanding interest

1. Spence MM, Rubin SM, Dimitrov IE, Ruiz EJ, Wemmer DE, Pines A, Yao SQ, Tian F, Schultz PG. Functionalized xenon as a biosensor. Proc Natl Acad Sci USA 2001;98:10654–10657. [PubMed: 11535830]
2. Lauterbur PC. Image formation by induced local interactions: examples employing nuclear magnetic resonance. Nature 1973;242:190–191.
3. Mansfield P, Grannell PK. NMR ‘diffraction’ in solids? J Phys C: Solid State Phys 1973;6:L422–L426.
4. Chan KW-Y, Wong W-T. Small molecular gadolinium(III) complexes as MRI contrast agents for diagnostic imaging. Coord Chem Rev 2007;251:2428–2451.

5. Slotkin J, Cahill K, Tharin S, Shapiro E. Cellular magnetic resonance imaging: Nanometer and micrometer size particles for noninvasive cell localization. Neurotherapeutics 2009;4:428–433. [PubMed: 17599708]
6. Urbanczyk-Pearson LM, Femia FJ, Smith J, Parigi G, Duimstra JA, Eckermann AL, Luchinat C, Meade TJ. Mechanistic investigation of beta-galactosidase-activated MR contrast agents. Inorg Chem 2008;47:56–68. [PubMed: 18072754]
7. Perez JM, Josephson L, Weissleder R. Use of magnetic nanoparticles as nanosensors to probe for molecular interactions. Chembiochem 2004;5:261–264. [PubMed: 14997516]
8. Mizukami S, Takikawa R, Sugihara F, Shirakawa M, Kikuchi K. Dual-function probe to detect protease activity for fluorescence measurement and ^{19}F MRI. Angew Chem-Int Ed 2009;48:3641–3643.
9. Mugler JP, Driehuys B, Brookeman JR, Cates GD, Berr SS, Bryant RG, Daniel TM, deLange EE, Downs JH, Erickson CJ, et al. MR imaging and spectroscopy using hyperpolarized Xe-129 gas: Preliminary human results. Magn Res Med 1997;37:809–815.
10. Golman K, Petersson JS. Metabolic imaging and other applications of hyperpolarized C- 13. Academic Radiol 2006;13:932–942.
11. Clevelanda ZI, Pavlovskayaa GE, Elkinsb ND, Stupica KF, Repineb JE, Meersmann T. Hyperpolarized ^{83}Kr MRI of lungs. J Magn Reson 2008;195:232–237. [PubMed: 18948043]
12. Hopkins SR, Levin DL, Emami K, Kadlecek S, Yu JS, Ishii M, Rizi RR. Advances in magnetic resonance imaging of lung physiology. J Appl Physiol 2007;102:1244–1254. [PubMed: 17158249]
13. Berthault P, Huber G, Desvaux H. Biosensing using laser-polarized xenon NMR/MRI. Prog Nucl Magn Reson Spec 2008;55:35–60.
14. Ruset IC, Ketel S, Hersman FW. Optical pumping system design for large production of hyperpolarized ^{129}Xe. Phys Rev Lett 2006;96 053002-053001-053004.
15. Clever, HL. Solubility Data Series. Vol. 2. New York: Pergamon Press; 1979.
16. Rathore R, Lindeman SV, Rao K, Sun D, Kochi JK. Guest penetration deep within the cavity of calix [4]arene hosts: The tight binding of nitric oxide to distal (cofacial) aromatic groups. Angew Chem-Int Ed 2000;39:2123–2127.
17. Bartik K, Luhmer M, Heyes SJ, Ottinger R, Reisse J. Probing molecular cavities in alpha-cyclodextrin solutions by xenon NMR. J Magn Reson B 1995;109:164–168.
18. Kim BS, Ko YH, Kim Y, Lee HJ, Selvapalam N, Lee HC, Kim K. Water soluble cucurbit[6]uril derivative as a potential Xe carrier for Xe-129 NMR-based biosensors. Chem Commun 2008:2756–2758.
19. Ripmeester JA, Ratcliffe CI, Tse JS. The nuclear magnetic-resonance of Xe-129 trapped in clathrates and some other solids. J Chem Soc-Faraday Trans I 1988;84:3731–3745.
20. Robbins TA, Knobler CB, Bellew DR, Cram DJ. Host-guest complexion .67. A highly adaptive and strongly binding hemicarcerand. J Am Chem Soc 1994;116:111–122.
21. Fukutomi J, Adachi Y, Kaneko A, Kimura A, Fujiwara H. Inclusion complex formation of thiacalix [4]arene and Xe in aqueous solution studied by hyperpolarized Xe-129 NMR. J Incl Phenom Macrocyclic Chem 2007;58:115–122.
22. Gabard J, Collet A. Synthesis of a (D3)-Bis(cyclotriveratrylenyl) macrocage by stereospecific replication of a (C3) -subunit. J Chem Soc-Chem Commun 1981:1137–1139.
23. Bartik K, Luhmer M, Dutasta J-P, Collet A, Reisse J. ^{129}Xe and ^{1}H NMR study of the reversible trapping of xenon by cryptophane-A in organic solution. J Am Chem Soc 1998;120:784–791.
24. Brotin T, Dutasta JP. Cryptophanes and their complexes--Present and future. Chem Rev 2009;109:88–130. [PubMed: 19086781]
25 •. Fogarty HA, Berthault P, Brotin T, Huber G, Desvaux H, Dutasta JP. A cryptophane core optimized for xenon encapsulation. J Am Chem Soc 2007;129:10332–10333. The authors report the smallest synthesized cryptophane cage, cryptophane-111, which exhibits the highest association constant to date for Xe in organic solvents, 10000 M^{-1} at 293 K. [PubMed: 17676741]
26. Mecozzi S, Rebek J. The 55% solution: A formula for molecular recognition in the liquid state. Chem Eur J 1998;4:1016–1022.
27 ••. Schroder L, Lowery TJ, Hilty C, Wemmer DE, Pines A. Molecular imaging using a targeted magnetic resonance hyperpolarized biosensor. Science 2006;314:446–449. A new technique,

hyper-CEST, was introduced to improve the hp ^{129}Xe MRI signal. Accumulation of depolarized nuclei occurs via selective saturation of biosensor-encapsulated ^{129}Xe and subsequent chemical exchange with the free xenon. [PubMed: 17053143]

28. Huber G, Brotin T, Dubois L, Desvaux H, Dutasta JP, Berthault P. Water soluble cryptophanes showing unprecedented affinity for xenon: Candidates as NMR-based biosensors. J Am Chem Soc 2006;128:6239–6246. [PubMed: 16669694]
29. Hill PA, Wei Q, Eckenhoff RG, Dmochowski IJ. Thermodynamics of xenon binding to cryptophane in water and human plasma. J Am Chem Soc 2007;129:9262–9263. [PubMed: 17616197]
30 •. Hill PA, Wei Q, Troxler T, Dmochowski IJ. Substituent effects on xenon binding affinity and solution behavior of water-soluble cryptophanes. J Am Chem Soc 2009;131:3069–3077. The highest association constant for xenon in buffer, $K_A \sim 33{,}000\ M^{-1}$ at 293 K, was obtained for cryptophane functionalized with three nearby carboxylates. [PubMed: 19239271]
31. Brotin T, Devic T, Lesage A, Emsley L, Collet A. Synthesis of deuterium-labeled cryptophane-A and investigation of Xe@Cryptophane complexation dynamics by 1D-EXSY NMR experiments. Chem Eur J 2001;7:1561–1573.
32. Spence MM, Ruiz EJ, Rubin SM, Lowery TJ, Winssinger N, Schultz PG, Wemmer DE, Pines A. Development of a functionalized xenon biosensor. J Am Chem Soc 2004;126:15287–15294. [PubMed: 15548026]
33 •. Schlundt A, Kilian W, Beyermann M, Sticht J, Guenther S, Höpner S, Falk K, Roetzschke O, Mitschang L, Freund C. A xenon-129 biosensor for monitoring MHC-peptide interactions. Angew Chem Int Ed Engl 2009;48:4142–4145. A major histocompatibility complex (MHC) class II protein was targeted with a specific peptide ligand attached to cryptophane-A. A chemical shift difference of approximately 1 ppm was reported between free and MHC-bound biosensors by hp ^{129}Xe NMR spectroscopy. [PubMed: 19408266]
34 •. Roy V, Brotin T, Dutasta J-P, Charles M-H, Delair T, Mallet F, Huber G, Desvaux H, Boulard Y, Berthault P. A cryptophane biosensor for the detection of specific nucleotide targets through xenon NMR spectroscopy. ChemPhysChem 2007;8:2082–2085. A cryptophane-DNA oligonucleotide biosensor was synthesized for *in vitro* DNA detection. The hp ^{129}Xe NMR spectrum showed that in the presence of the complementary strand, the bound xenon signal was shifted upfield by ~1.5 ppm, whereas it remained unchanged in the presence of the non-complementary strand. [PubMed: 17712828]
35 ••. Seward GK, Wei Q, Dmochowski IJ. Peptide-mediated cellular uptake of cryptophane. Bioconj Chem 2008;19:2129–2135. Cellular delivery of cryptophane into human cancer and normal cell lines was first reported. Peptide-labeled cryptophanes were determined to be relatively nontoxic by MTT assay at the micromolar concentrations required for hp ^{129}Xe NMR experiments. A tetra (RGD)-functionalized cryptophane showed cell uptake mediated by integrin.
36 ••. Chambers JM, Hill PA, Aaron JA, Han ZH, Christianson DW, Kuzma NN, Dmochowski IJ. Cryptophane xenon-129 nuclear magnetic resonance biosensors targeting human carbonic anhydrase. J Am Chem Soc 2009;131:563–569. Biosensors complexed with CA I and II yielded "bound" hyperpolarized ^{129}Xe NMR resonances of narrow linewidth that were shifted between 3.0 and 7.5 ppm downfield compared to the "free" biosensor. The NMR spectra clearly distinguished between CA I and II in solution. [PubMed: 19140795]
37. Wei Q, Seward GK, Hill PA, Patton B, Dimitrov IE, Kuzma NN, Dmochowski IJ. Designing Xe-129 NMR biosensors for matrix metalloproteinase detection. J Am Chem Soc 2006;128:13274–13283. [PubMed: 17017809]
38. Duhamel G, Choquet P, Grillon E, Lamalle L, Leviel JL, Ziegler A, Constantinesco A. Xenon-129 MR imaging and spectroscopy of rat brain using arterial delivery of hyperpolarized xenon in a lipid emulsion. Magn Reson Med 2001;46:208–212. [PubMed: 11477622]
39. Ruppert K, Mata JF, Brookeman JR, Hagspiel KD, Mugler JP. Exploring lung function with hyperpolarized Xe-129 nuclear magnetic resonance. Magn Reson Med 2004;51:676–687. [PubMed: 15065239]
40. Driehuys B, Cofer GP, Pollaro J, Mackel JB, Hedlund LW, Johnson GA. Imaging alveolar-capillary gas transfer using hyperpolarized Xe-129 MRI. Proc Natl Acad Sci USA 2006;103:18278–18283. [PubMed: 17101964]

41 ••. Driehuys B, Pollaro J, Cofer GP. In vivo MRI using real-time production of hyperpolarized Xe-129. Magn Res Med 2008;60:14–20. ^{129}Xe MRI was successfully applied to evaluate pulmonary perfusion or gas exchange in the lung of rats, using intravenously injected hp ^{129}Xe-saturated saline.

42. Goodson BM, Song YQ, Taylor RE, Schepkin VD, Brennan KM, Chingas GC, Budinger TF, Navon G, Pines A. In vivo NMR and MRI using injection delivery of laser-polarized xenon. Proc Natl Acad Sci USA 1997;94:14725–14729. [PubMed: 9405680]

43. Venkatesh AK, Zhao L, Balamore D, Jolesz FA, Albert MS. Evaluation of carrier agents for hyperpolarized xenon MRI. NMR Biomed 2000;13:245–252. [PubMed: 10867704]

44. Luhmer M, Goodson BM, Song YQ, Laws DD, Kaiser L, Cyrier MC, Pines A. Study of xenon binding in cryptophane-A using laser-induced NMR polarization enhancement. J Am Chem Soc 1999;121:3502–3512.

45. Cherubini A, Bifone A. Hyperpolarised xenon in biology. Prog Nucl Magn Reson Spec 2003;42:1–30.

46. Wolber J, Rowland IJ, Leach MO, Bifone A. Perfluorocarbon emulsions as intravenous delivery media for hyperpolarized xenon. Magn Reson Med 1999;41:442–449. [PubMed: 10204864]

47. Bifone A, Song YQ, Seydoux R, Taylor RE, Goodson BM, Pietrass T, Budinger TF, Navon G, Pines A. NMR of laser-polarized xenon in human blood. Proc Natl Acad Sci USA 1996;93:12932–12936. [PubMed: 8917521]

48. Welsh RC, Chupp TE, Coulter KP, Rosen MS, Swanson SD. Magnetic resonance imaging with laser-polarized Xe-129. Nucl Instrum Methods Phys Res A-Accel Spectrom Det Assoc Equip 1998;402:461–463.

49. Marx T, Schmidt M, Schirmer U, Reinelt H. Xenon anaesthesia. J R Soc Med 2000;93:513–517. [PubMed: 11064688]

50. Mynar JL, Lowery TJ, Wemmer DE, Pines A, Frechet JMJ. Xenon biosensor amplification via dendrimer-cage supramolecular constructs. J Am Chem Soc 2006;128:6334–6335. [PubMed: 16683795]

51. Mulder WJM, Strijkers GJ, van Tilborg GAF, Griffioen AW, Nicolay K. Lipid-based nanoparticles for contrast-enhanced MRI and molecular imaging. NMR Biomed 2006;19:142–164. [PubMed: 16450332]

52 •. Lerouge F, Melnyk O, Durand JO, Raehm L, Berthault P, Huber G, Desvaux H, Constantinesco A, Choquet P, Detour J, et al. Towards thrombosis-targeted zeolite nanoparticles for laser-polarized Xe-129 MRI. J Mater Chem 2009;19:379–386. Very slow exchange phenomenon between free xenon and xenon embedded in pores of zeolite colloidal nanoparticles functionalized with a peptide is observed and hp ^{129}Xe exhibits fairly long relaxation times inside the pores. This is the first paper to look at the distribution of a xenon biosensor *in vivo*.

53. Harel E, Schroder L, Xu S. Novel detection schemes of nuclear magnetic resonance and magnetic resonance imaging: Applications from analytical chemistry to molecular sensors. Annu Rev Anal Chem 2008;1:133–163.

54. Lowery TJ, Garcia S, Chavez L, Ruiz EJ, Wu T, Brotin T, Dutasta JP, King DS, Schultz PG, Pines A, et al. Optimization of xenon biosensors for detection of protein interactions. Chembiochem 2006;7:65–73. [PubMed: 16342304]

55. Ruiz EJ, Sears DN, Pines A, Jameson CJ. Diastereomeric Xe chemical shifts in tethered cryptophane cages. J Am Chem Soc 2006;128:16980–16988. [PubMed: 17177449]

56. Moule AJ, Spence MM, Han SI, Seeley JA, Pierce KL, Saxena S, Pines A. Amplification of xenon NMR and MRI by remote detection. Proc Natl Acad Sci USA 2003;100:9122–9127. [PubMed: 12876195]

57. Sears DN, Jameson CJ. Theoretical calculations of the Xe chemical shifts in cryptophane cages. J Chem Phys 2003;119:12231–12244.

58 •. Aaron JA, Chambers JM, Jude KM, Costanzo LD, Dmochowski IJ, Christianson DW. Structure of a ^{129}Xe-cryptophane biosensor complexed with human carbonic anhydrase II. J Am Chem Soc 2008;130:6942–6943. The first reported X-ray crystal structure of cryptophane bound to protein (CA) confirms tight binding of biosensor with CAII and the encapsulation of one xenon atom inside of functionalized cryptophane. [PubMed: 18461940]

59. Schröder L, Chavez L, Meldrum T, Smith M, Lowery TJ, Wemmer DE, Pines A. Temperature-controlled molecular depolarization gates in nuclear magnetic resonance. Angew Chem-Int Ed 2008;47:4316–4320.

60. Hilty C, Lowery TJ, Wemmer DE, Pines A. Spectrally resolved magnetic resonance imaging of a xenon biosensor. Angew Chem-Int Ed 2006;45:70–73.

61 •. Berthault P, Bogaert-Buchmann A, Desvaux H, Huber G, Boulard Y. Sensitivity and multiplexing capabilities of MRI based on polarized Xe-129 biosensors. J Am Chem Soc 2008;130:16456–16457. Discrimination via high spatial resolution ^{129}Xe MRI images was achieved between xenon in two different hosts dissolved in two immiscible media by using a gradient echo sequence with interleaved frequency selection. [PubMed: 19554716]

62. Driehuys B, Moller HE, Cleveland ZI, Pollaro J, Hedlund LW. Pulmonary perfusion and xenon gas exchange in rats: MR imaging with intravenous injection of hyperpolarized Xe-129. Radiology 2009;252:386–393. [PubMed: 19703880]

63. Santyr GE, Lam WW, Parra-Robles JM, Taves TM, Ouriadov AV. Hyperpolarized noble gas magnetic resonance imaging of the animal lung: Approaches and applications. J Appl Phys 2009;105:102004.

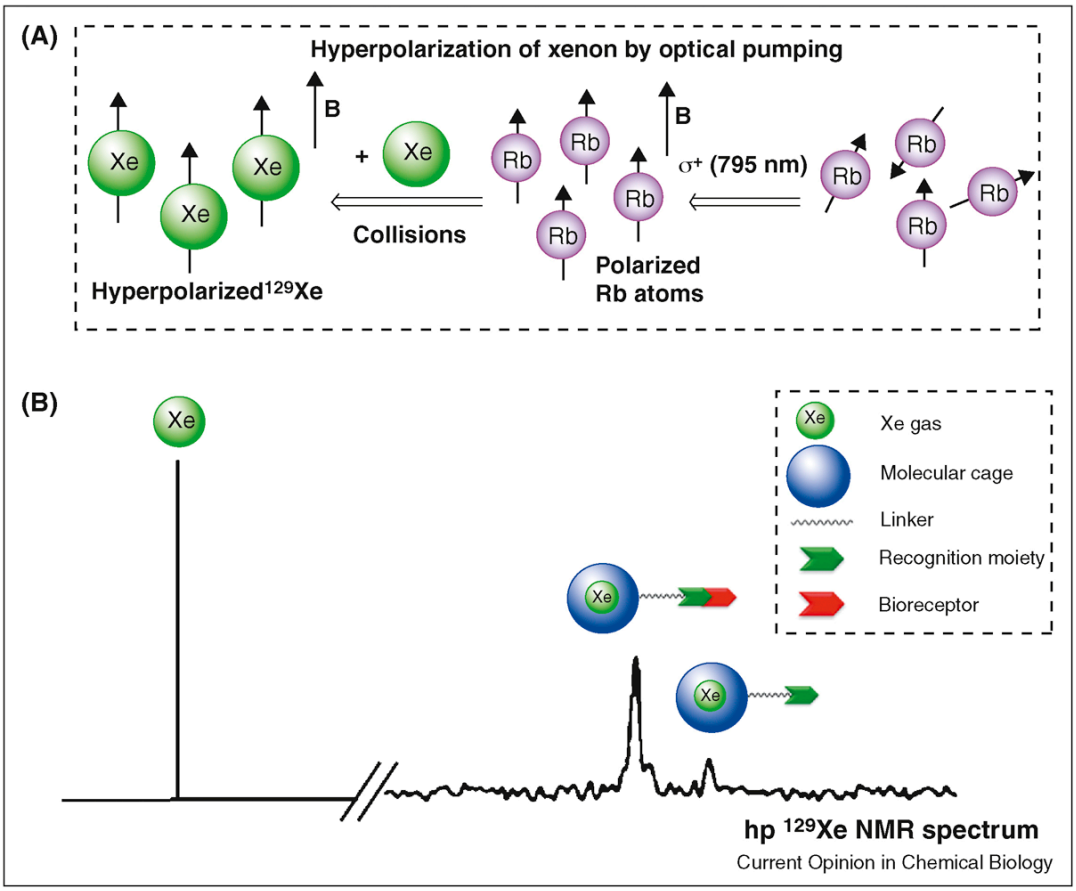

Figure 1.

A) Process of optical pumping to produce hyperpolarized ^{129}Xe. **B)** Schematic representation of hp ^{129}Xe NMR spectrum showing (from left) resonances of free xenon gas in aqueous solution, Xe-encapsulated biosensor bound to corresponding bioreceptor, and Xe encapsulated in free biosensor. Legend shows components of biosensor: molecular cage, linker, and recognition moiety.

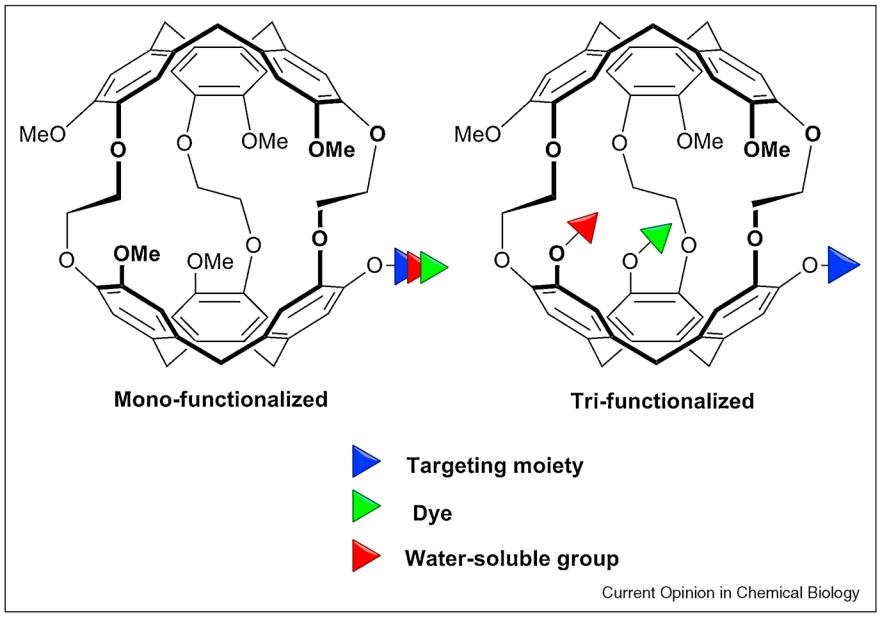

Figure 2.
Alternate mono- and tri-functionalization approaches for attaching targeting moieties, dye molecules, and water-solubilizing groups to cryptophane-A.

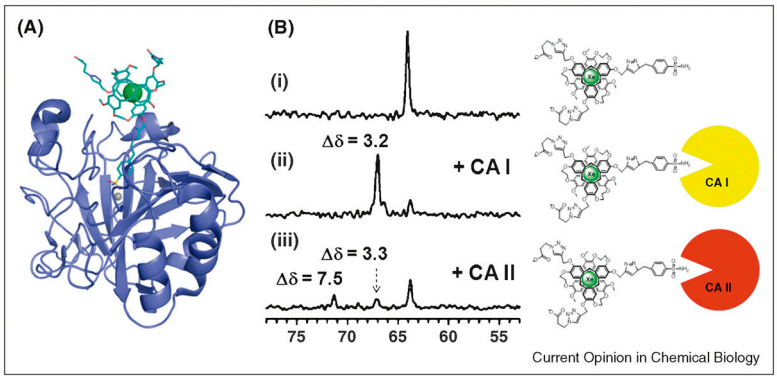

Figure 3.

A) X-ray crystal structure of CAII bound to benzenesulfonamide-8-bond-linker cryptophane, only one enantiomer shown. Data reveal sulfonamidate coordination to Zn^{2+} (gray atom), and Xe (green atom) bound inside cryptophane. **B)** Laser-polarized ^{129}Xe NMR spectra: (i) 7-bond-linker biosensor free in solution; (ii) biosensor bound to CAI and (iii) CAII.

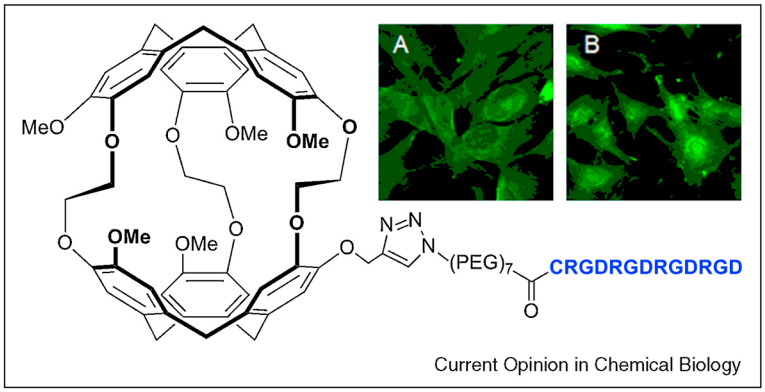

Figure 4.
Cryptophane-tetraRGD biosensor targeting $\alpha_v\beta_3$ integrin. Inset: Uptake of Cy3-labeled biosensor in (A) NCI-H1975 and (B) HFL-1 cells.